MCB
Journals.ASM.org

Sept6 Is Required for Ciliogenesis in Kupffer's Vesicle, the Pronephros, and the Neural Tube during Early Embryonic Development

Gang Zhai,[a,b] Qilin Gu,[a,b] Jiangyan He,[a] Qiyong Lou,[a] Xiaowen Chen,[a] Xia Jin,[a] Erfei Bi,[c] Zhan Yin[a]

Key Laboratory of Aquatic Biodiversity and Conservation, Institute of Hydrobiology, Chinese Academy of Science, Wuhan, Hubei, People's Republic of China[a]; Graduate School of the Chinese Academy of Science, Beijing, People's Republic of China[b]; Department of Cell and Developmental Biology, University of Pennsylvania Perelman School of Medicine, Philadelphia, Pennsylvania, USA[c]

Septins are conserved filament-forming GTP-binding proteins that act as cellular scaffolds or diffusion barriers in a number of cellular processes. However, the role of septins in vertebrate development remains relatively obscure. Here, we show that zebrafish *septin 6* (*sept6*) is first expressed in the notochord and then in nearly all of the ciliary organs, including Kupffer's vesicle (KV), the pronephros, eye, olfactory bulb, and neural tube. Knockdown of *sept6* in zebrafish embryos results in reduced numbers and length of cilia in KV. Consequently, cilium-related functions, such as the left-right patterning of internal organs and nodal/spaw signaling, are compromised. Knockdown of *sept6* also results in aberrant cilium formation in the pronephros and neural tube, leading to cilium-related defects in pronephros development and Sonic hedgehog (Shh) signaling. We further demonstrate that SEPT6 associates with acetylated α-tubulin *in vivo* and localizes along the axoneme in the cilia of zebrafish pronephric duct cells as well as cultured ZF4 cells. Our study reveals a novel role of *sept6* in ciliogenesis during early embryonic development in zebrafish.

Septins are a conserved family of GTP-binding proteins that play important roles in diverse cellular functions, including cell cycle progression, vesicle trafficking, cytokinesis, cell migration, membrane dynamics, and chromosome segregation (1–8). They are also important for maintaining polarized membrane domains by acting as diffusion barriers at the neck region of the budding yeast *Saccharomyces cerevisiae*, the annulus of spermatozoa, and the base of dendritic spines or primary cilia (9–14). Septins typically consist of four conserved domains: a phospholipid-binding polybasic (PB) region, a GTP-binding domain (GTPase), a septin-unique element (SUE), and a coiled-coil (CC) domain (except for the SEPT3 subgroup) (15). Based on similarities in amino acid sequences, septins are classified into four subgroups: the SEPT2 subgroup (SEPT1, SEPT2, SEPT4, and SEPT5), the SEPT3 subgroup (SEPT3, SEPT9, and SEPT12), the SEPT6 subgroup (SEPT6, SEPT8, SEPT10, SEPT11, and SEPT14), and the SEPT7 subgroup (SEPT7) (15–17).

Septins in different organisms form apolar, rod-shaped, heterooligomeric complexes that polymerize end to end into linear filaments (18). Previously, at least three mammalian complexes (SEPT4/5/8, SEPT7/9b/11, and SEPT2/6/7) have been characterized, and septin subunits have been shown to be symmetrically arranged (e.g., SEPT7-SEPT6-SEPT2-SEPT2-SEPT6-SEPT7) in the complexes. These complexes are thought to assemble into filaments through an interaction between the guanine nucleotide-binding domains (G interface) of the terminal subunits in the neighboring septin complexes (19, 20). More recent studies have indicated that mammalian septins form heterooctameric complexes, with two copies of a subunit from each of the septin subgroups (e.g., SEPT9-SEPT7-SEPT6-SEPT2-SEPT2-SEPT6-SEPT7-SEPT9), similar to the octameric septin complexes in *Saccharomyces cerevisiae* (21, 22). These septin complexes are thought to form filaments through interactions between the N- and C-terminal domains (NC interface) of the terminal subunits in the neighboring septin complexes (23, 24).

SEPT2 in mouse inner medullary collecting duct (IMCD3) cells and SEPT7 in *Xenopus laevis* multiciliated cells are found to form ring-like structures at the base of primary cilia, a microtubule-based organelle that plays important roles in a wide range of cellular processes in different biological systems (13, 25). Depletion of SEPT2 or SEPT7 causes defects in ciliogenesis. These septin rings are thought to act as diffusion barriers for maintaining distinct membrane domains. Recently, SEPT2/7/9 were reported to localize along the axoneme in the primary cilia of retinal pigmented epithelial (RPE) cells and to regulate ciliary length (26). However, the role of septins in ciliogenesis in the context of vertebrate development has not been extensively explored.

In recent years, the function of cilia in vertebrate organogenesis has been a focus of study, as disruption of cilium structure or function has been linked to a number of human diseases and disorders, including blindness, mental retardation, obesity, etc. (27–29). Polycystic kidney disease (PKD) has been linked to defective cilia in kidney tubules (30–36). In mice, cilia in the node, which is the counterpart of the Kupffer's vesicle (KV) in zebrafish, are involved in the initiation of left-right (LR) asymmetry by generating a counterclockwise fluid flow to break the bilateral symmetry of the gastrulating embryo (36–40). In addition, mutants deficient in

Received 25 October 2013 Returned for modification 30 November 2013
Accepted 21 January 2014
Published ahead of print 27 January 2014
Address correspondence to Zhan Yin, zyin@ihb.ac.cn, or Erfei Bi, ebi@mail.med.upenn.edu.

doi:10.1128/MCB.01409-13

TABLE 1 Primers used in this study

Assay and primer target gene	Primer direction[a]	Primer sequence (5′–3′)
RT-PCR: *sept6*	F	CGGCCACTGAGATAGCACGACAA
	R	CATCTGATTTGGCAATGATGGG
Real-time PCR		
shh	F	TACGAGGGCAAGATAACGC
	R	ACAGAGATGGCCAGCGAG
nkx2.2	F	CAGCATCCAATACTCATTACAC
	R	CTTCTTACCAGAGTCGCTG
gli1	F	CTACCAGCTCTCTCAGCAAC
	R	GCAGGACATTCCAGTGACTC
ptch1	F	CAGAGTTTGACTTCATCATGAG
	R	CGTTGTTAGCAGGTACAACC
β-*actin*	F	CGGAATATCATCTGCTTGTAA
	R	CATCATCTCCAGCGAATC

[a] F, forward; R, reverse.

ciliary components also display retinal dystrophy and neurological problems (41–44).

Mammalian SEPT6 is a fusion partner of the mixed-lineage leukemia (MLL) gene in acute myeloid leukemia patients (45). However, *sept6*-deficient mice did not show any detectable phenotype (46). Deletion of SEPT6 also did not affect leukemogenesis induced by MLL-SEPT6. Thus, the role of SEPT6, though expressed ubiquitously in mammalian tissues, remains unknown.

In this study, the zebrafish model was employed for function analysis of SEPT6. We found that *sept6* is expressed in the ciliated organs, such as the KV, pronephros, eye, olfactory bulb, and neural tube, in developing zebrafish embryos. Knockdown of *sept6* by two independent morpholino oligonucleotides (MOs) leads to reduced numbers and lengths of cilia in the KV, pronephros, and neural tube, which causes aberrant phenotypes, including reversed LR patterning of internal organs, cyst formation and dilated tubules and ducts in the pronephros, and impaired Shh signaling. Strikingly, these developmental phenotypes closely resemble those of zebrafish mutants deficient in ciliary components, such as the proteins involved in intraflagellar transport (IFTs) (36). Thus, our study provides strong evidence for the role of *sept6* in controlling ciliogenesis in zebrafish.

MATERIALS AND METHODS

Zebrafish maintenance. Wild-type (AB) zebrafish (*Danio rerio*) were raised and maintained under standard conditions at 28.5°C (47). Developmental stages of zebrafish embryos were characterized as described previously (48).

RT-PCR. To examine the expression of *sept6*, total RNA was extracted from zebrafish embryos by using TRIzol (15596-026; Invitrogen), and single-stranded cDNA was synthesized using an oligo(dT)$_{18}$ primer and the RevertAid first-strand cDNA synthesis kit (K1622; Thermo Scientific) according to the manufacturer's instructions. Reverse transcription-PCR (RT-PCR) primers for *sept6* expression were designed by using the software Primer 5.0 and are listed in Table 1.

RNA and morpholino injection. The full length of zebrafish *sept6* was cloned into vector pSP64 (Promega), and the capped *sept6* mRNA was synthesized using the mMESSAGE mMACHINE SP6 kit (AM1340; Ambion) according to the manufacturer's instructions. Three morpholinos were purchased from Gene Tool Company: *sept6*-tMO, targeting the translation start codon site of *sept6* (5′-CATGGTTCTCTCCTGCATCAAA CCT-3′), *sept6*-sMO, targeting the splicing site between exon 2 and intron 2 (5′-CTCCCACATGACACACTCACCCCA-3′), and standard MO (std-MO; 5′-CCTCTTACCTCAGTTACAATTTATA-3′). MOs and mRNA were injected into 1- or 2-cell-stage embryos at nominated concentrations by using a *PLI-100A* microinjector (Harvard Medical Apparatus).

Whole-mount *in situ* hybridization. We carried out whole-mount *in situ* hybridization (WISH) as described previously (49). cDNAs of the following genes were used as antisense probes in our study: *sept6*, *ceruloplasmin* (*cp*), *forkhead box A3* (*foxa3*), *cardiac myosin light chain 2* (*cmlc2*), *southpaw* (*spaw*), *lefty1*, *lefty2*, *no tail* (*ntl*), *charon*, *SRY-box containing gene 17* (*sox17*), *sonic hedgehog* (*shh*), *gliotactin 1* (*gli1*), *NK2 homeobox 2* (*nkx2.2*), and *patched 1* (*ptch1*).

Immunofluorescence. Immunofluorescence using mouse anti-acetylated α-tubulin antibody (T6793; Sigma) and rabbit antihemagglutinin (anti-HA) antibody (H6908; Sigma) was carried out as described before (50, 51). Confocal images of the embryos and ZF4 cells were taken with 40× and 100× objective lenses, respectively, of a NOL-LSM 710 microscope (Carl Zeiss, Germany). The numbers and lengths of KV cilia were measured by using NIH ImageJ software. Statistical analysis was performed using Student's *t* test of the Statistical Program for Social Sciences (SPSS). Every result represents the mean of at least three independent experiments.

Coimmunoprecipitation. The association between zebrafish acetylated α-tubulin and SEPT6 (sc-20180; Santa Cruz Biotechnology) was determined using the Pierce coimmunoprecipitation (co-IP) kit (26149; Thermo Scientific), following the instructions of the manufacturer.

FCF treatment. Forchlorfenuron (FCF; 32974; $C_{12}H_{10}ClN_3O$; Sigma) is a septin inhibitor that affects septin assembly and organization (52, 53). Wild-type embryos were cultured in the presence of 150 μM FCF from 70% epiboly to the prim-5 stage. WISH at 2 days postfertilization (dpf) and immunofluorescence at the 8-somite (ss) stage were then performed to assess the liver patterning and KV ciliogenesis of the FCF- and dimethyl sulfoxide (DMSO)-treated embryos.

Real-time PCR. To determine the expression levels of the Shh signaling factors, real-time PCR was performed on embryos at 24 h postfertilization (hpf). Total RNA extraction and cDNA synthesis were carried out as described above. SYBR green real-time PCR master mix (QPK-212; Toyobo) was used for PCR in a real-time detection system (Bio-Rad). Primers for *shh*, *nkx2.2*, *gli1*, and *ptch1* were designed using the software Primer 5.0 and are listed in Table 1.

RESULTS

Identification of *sept6* in zebrafish. The putative zebrafish *sept6* is located on chromosome 14 (GenBank accession number BC056592.1, NCBI) and encodes a protein of 427 amino acids. Like all other septins, zebrafish SEPT6 is a GTP-binding protein with conserved motifs (G1, G3, G4, S1, S2, and S3) in the nucleotide-binding site (Fig. 1A) (54–56). It also contains a predicted coiled-coil region in its C terminus, a common feature among many septins (55). Similar to its mammalian counterpart, zebrafish SEPT6 lacks the critical threonine (Thr) residue corresponding to Thr-78 in mouse SEPT2, which is required for GTP hydrolysis (20, 55).

Phylogenetic analysis using the software MEGA 5.05 indicated that zebrafish SEPT6 has closest homology to SEPT6 from *Homo sapiens*, *Mus musculus*, and *Xenopus laevis* (Fig. 1B). Chromosome linkage analysis using tools on the Genomicus website (http://www.dyogen.ens.fr/genomicus-67.01/cgi-bin/search.pl) indicated that zebrafish *sept6* is linked to the *NKRF*, *UBE2A*, *SLC25A43*, and *SLC25A5* loci, similar to *sept6* in *Homo sapiens*, *Mus musculus*, and *Xenopus laevis* (Fig. 1C). Taken together, these features suggest that zebrafish *sept6* is the orthologue of mammalian *sept6*.

***sept6* is involved in body morphogenesis during zebrafish development.** To explore the *in vivo* role of *sept6*, we first exam-

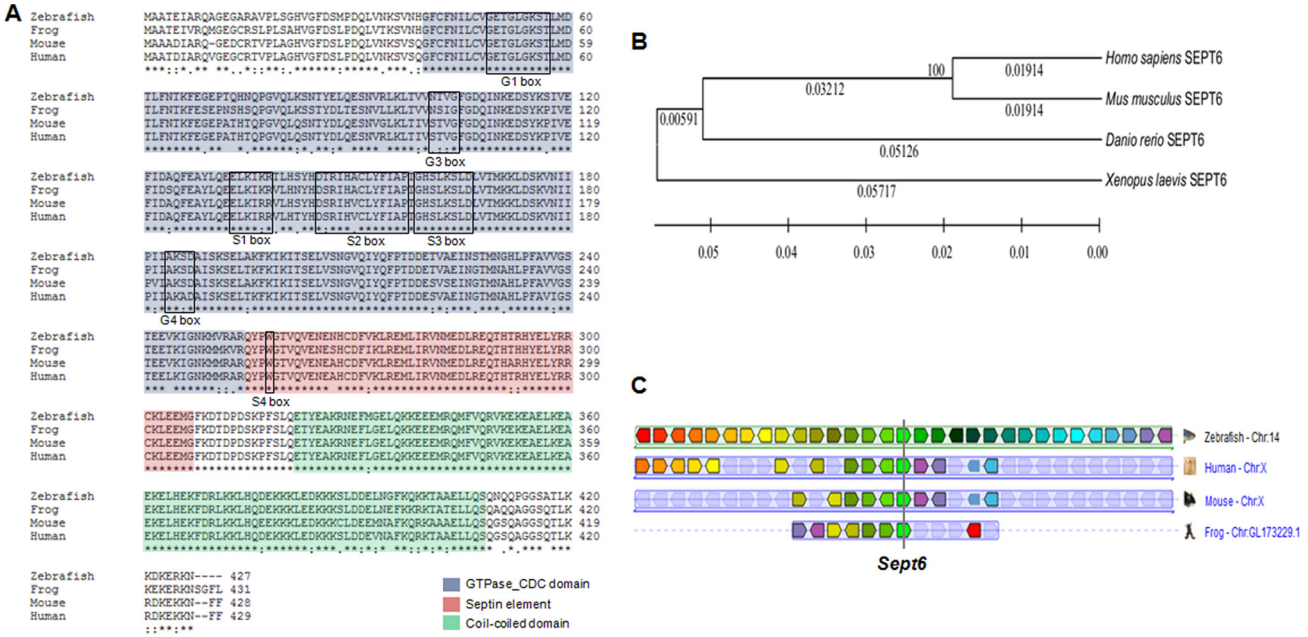

FIG 1 Zebrafish SEPT6. (A) Alignment of amino acid sequences of SEPT6 from human (Uniprot accession number Q14141.4), mouse (Q9R1T4.4), frog (AAH77941.1), and zebrafish (AAH56592.1). The GTPase CDC domain, septin unique element, and coiled-coil domain are highlighted in different colors. The G1, G3, G4, S1, S2, S3, and S4 motifs are boxed. (B) Phylogenetic analysis of amino acid sequences from the indicated species. The distance scale represents the degree of difference between sequences (e.g., 0.1 indicates a 10% difference between two sequences). (C) Chromosome linkage analysis of *sept6* from the indicated species.

ined its expression pattern during early embryonic development. As shown by RT-PCR analysis, *sept6* was expressed throughout embryogenesis (Fig. 2A). WISH analysis further indicated that maternally derived *sept6* transcript was distributed ubiquitously prior to the shield stage (Fig. 2B to D). During the early segmentation stage, the expression of *sept6* was restricted to the notochord, KV, and spinal cord neurons (Fig. 2E to I). From the prim-15 to the long-pec stage, *sept6* RNA was localized in olfactory bulb, lens, inner nuclear layer, glomerulus, pronephric tubules, pronephric ducts, and neural tube (Fig. 2J to M). These

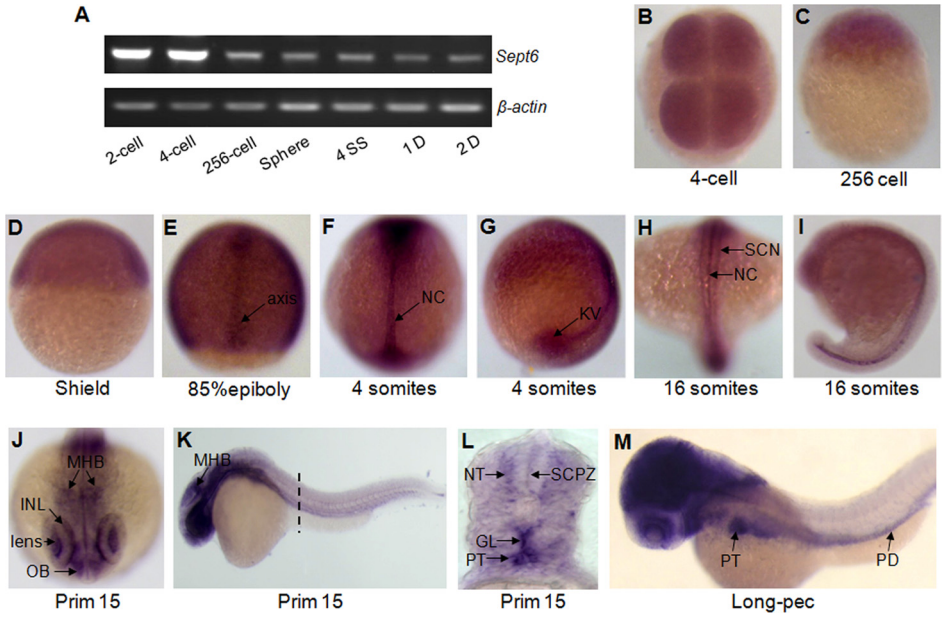

FIG 2 Expression patterns of *sept6* during zebrafish embryonic development. (A) Expression patterns of *sept6* at different stages were assessed by RT-PCR, with β-*actin* as the control. (B to M) WISH analysis of zebrafish *sept6* expression levels at different developmental stages. (B) Four-cell stage, top view; (C) 256-cell stage, lateral view; (D) shield stage, lateral view; (E) 85% epiboly stage, dorsal view; (F) 4-ss stage, dorsal view; (G) 4-ss stage, lateral view; (H) 16-ss stage, dorsal view; (I) 16-ss stage, lateral view; (J) prim-15 stage, front view; (K) prim-15, lateral view; (L) prim-15, cross-section view; (M) long-pec stage, lateral view. Abbreviations: NC, notochord; SCN, spinal cord neuron; MHB, midhindbrain boundary; INL, inner nuclear layer; OB, olfactory bulb; NT, neural tube; SCPZ, spinal cord proliferative zone; GL, glomerulus; PT, pronephric tubule; PD, pronephric duct.

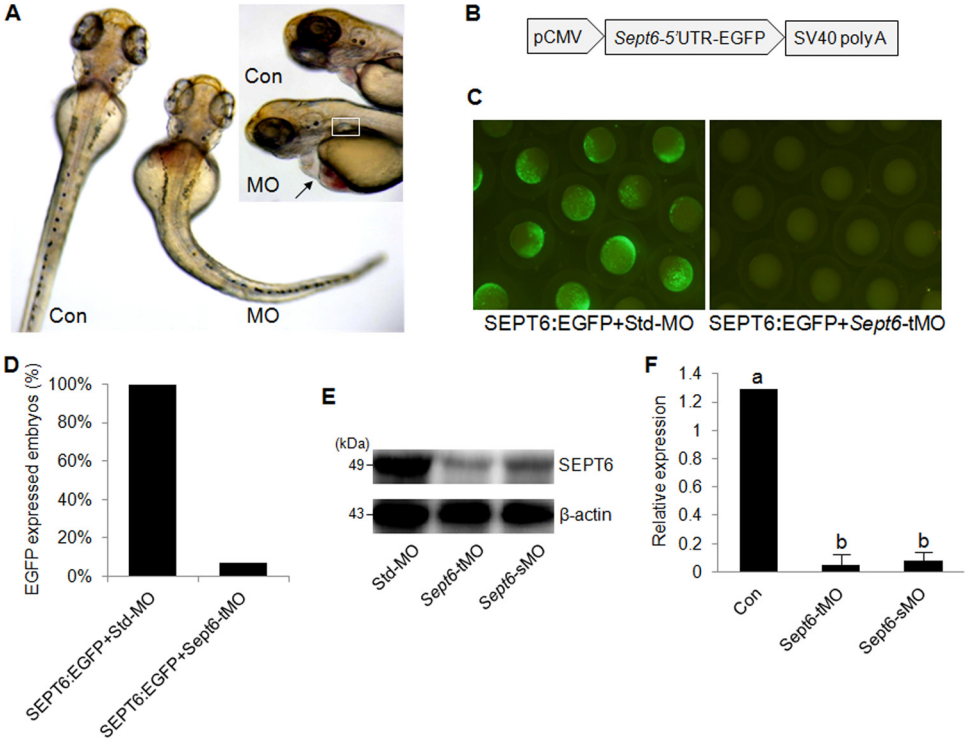

FIG 3 Global defects caused by *sept6* knockdown and specificity tests for MOs. (A) Representative images of control embryos (Con) and morphant (MO) embryos. Arrow, heart pericardium; square, pronephric cyst. The enlarged images of the brain area are shown in the inset. (B) Diagram of the construct containing the *sept6* 5′-UTR fused with EGFP and a simian virus 40 poly(A) tail, which is driven by the CMV promoter. (C) Representative images of embryos coinjected with the plasmid and *sept6*-tMO or std-MO. (D) Quantification of EGFP-expressing embryos from panel C. (E) Protein levels of SEPT6 in the control embryos, tMO morphants, and sMO morphants at 24 hpf. (F) Quantification of relative expression levels of SEPT6 from the Western blot shown in panel E. The expression levels of SEPT6 were normalized against β-actin. The letters a and b represent statistically significant differences ($P < 0.001$, calculated by using Student's *t* test).

results demonstrate that *sept6* is mainly expressed in the ciliary organs during zebrafish development.

Next, we determined the consequences of *sept6* knockdown during zebrafish embryonic development. Two MOs, one designed to block translation and one to block splicing, were used in this analysis. Embryos injected with either *sept6*-tMO or *sept6*-sMO, which are called morphants, had severe developmental defects, including curvature of the body, large pericardial effusion, and pronephric cyst (Fig. 3A). These knockdown effects, together with the expression patterns, suggested that *sept6* plays an important role in body morphogenesis during zebrafish development.

sept6-tMO targets the start codon AUG, and *sept6*-sMO targets the exon 2-intron 2 boundary. The specificity of *sept6*-tMO was demonstrated by injecting embryos with *sept6*-tMO and a plasmid carrying the cytomegalovirus (CMV) promoter-driven *sept6* 5′ untranslated region (UTR)-enhanced green fluorescent protein (EGFP) fusion, which contains the *sept6*-tMO target sequence in the 5′-UTR (Fig. 3B). Only 7.1% of the *sept6*-tMO morphants ($n = 56$) were positive for EGFP signal, in comparison to 100.0% of the control embryos (std-MO; $n = 55$) (Fig. 3C and D). Western blot analysis demonstrated that the expression of *sept6* was significantly reduced in the *sept6*-tMO and *sept6*-sMO morphants compared with the control embryos ($P < 0.001$) (Fig. 3E and F). These results indicated that *sept6*-tMO and *sept6*-sMO effectively block the expression of *sept6* in the morphants.

***sept6* affects LR patterning of visceral organs.** To further define the developmental role of *sept6*, we examined visceral organs during embryogenesis in the *sept6* morphants. By using the liver-specific marker *cp*, we found that 72.7% of the *sept6*-tMO ($n = 33$) and 61.2% of the *sept6*-sMO ($n = 21$) morphants showed laterality defects, compared with only 3.8% of embryos injected with the std-MO ($n = 25$) at 60 hpf (Fig. 4A to D). By using the endoderm marker *foxa3* for the primordial liver, pancreas, and gut, we found that 97.8% of the control embryos ($n = 93$) showed normal organ patterning at 60 hpf, i.e., the liver on the left side and the pancreas on the right side (Fig. 4E). In contrast, 56.3% of the *sept6*-tMO ($n = 135$) and 47.2% of the *sept6*-sMO ($n = 72$) morphants displayed inverted patterning (Fig. 4F and H). When embryos were coinjected with *sept6*-tMO and *sept6* mRNA or with *sept6*-sMO and *sept6* mRNA, only 23.8% of the *sept6*-tMO ($n = 80$) and 19.0% of the *sept6*-sMO ($n = 84$) morphants exhibited the inverted patterning (Fig. 4G and H). This partial rescue of the patterning defect by the *sept6* mRNA indicates that the observed phenotypes are specific to *sept6* knockdown. We also monitored the heart patterning with the *cmlc2* probe in embryos at 48 hpf, and we found that 95.4% of the control embryos ($n = 65$) showed normal patterning, i.e., the heart with a normal loop (Fig. 4I). In contrast, 57.7% of the *sept6*-tMO ($n = 52$) and 41.9% of the *sept6*-sMO ($n = 62$) morphants showed abnormal patterning, including hearts without a loop or with an inverted loop (Fig. 4J to L). When embryos were coinjected with *sept6*-tMO and *sept6* mRNA or with *sept6*-sMO and *sept6* mRNA, only 30.4% of the *sept6*-tMO ($n = 56$) and 17.9% of the *sept6*-sMO ($n = 56$) morphants showed abnormal patterning (Fig. 4J to L). Together, these data indicate

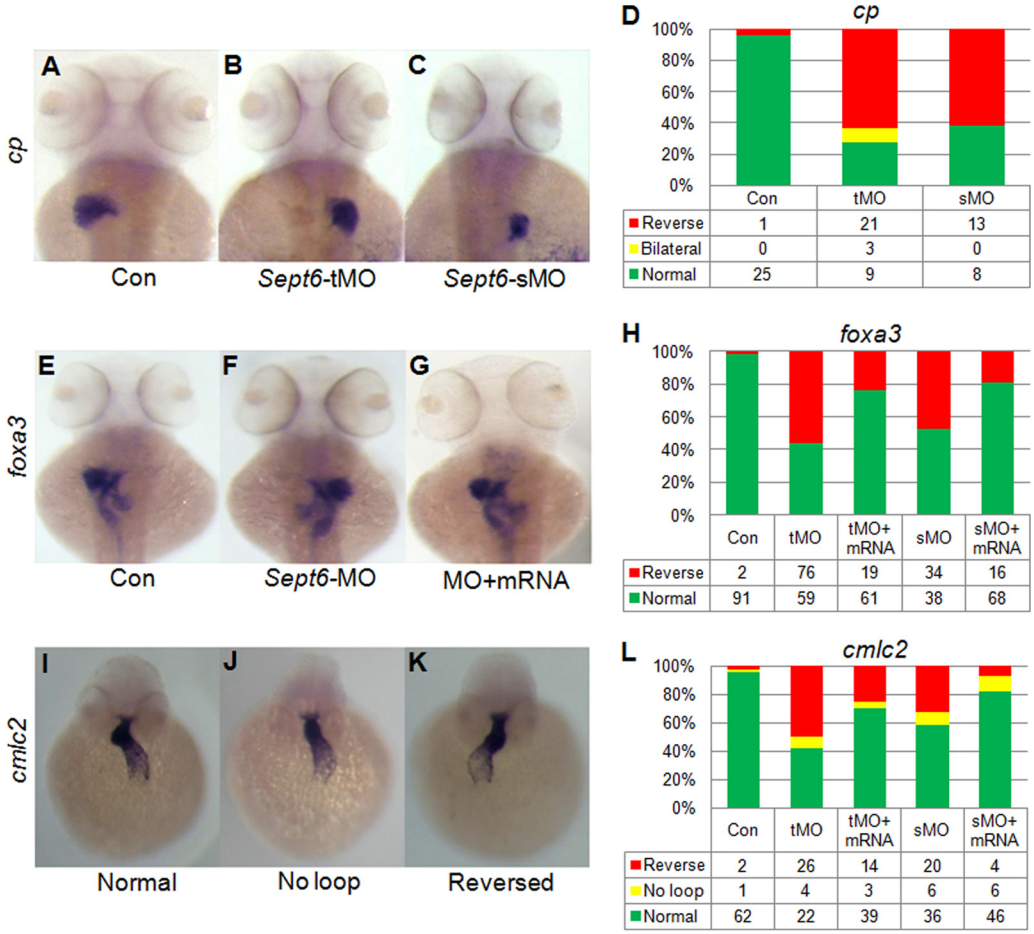

FIG 4 *sept6* is required for the LR patterning of visceral organs. *sept6*-tMO and sMO both caused aberrant patterns of liver (B and C), liver, pancreas, and gut (F), and heart (J and K), compared with the std-MO (A, E, and I). (G) Defective LR patterning of liver, pancreas, and gut in *sept6* morphants rescued by wild-type *sept6* mRNA coinjection. Percentages of the defective for the indicated gene and rescued embryos were quantified and are presented in the bar charts (D, H, and L).

that *sept6* is required for LR patterning of visceral organs during the hatch stage.

***sept6* is required for LR patterning of nodal signaling.** Nodal signaling in the lateral plate mesoderm (LPM) is critically important for situs-specific organogenesis in mammalian embryos (37, 57–59). To determine whether *sept6* affects LR asymmetry of visceral organs by controlling nodal signaling, we examined the effects of *sept6* knockdown on the expression patterns of the zebrafish nodal gene *spaw* and its downstream targets, *lefty1* and *lefty2*. As expected, in the control embryos *spaw* was expressed at the left side of the LPM (Fig. 5A). In contrast, aberrant expression patterns of *spaw*, including bilateral (Fig. 5B) and reversed (Fig. 5C) patterns, were observed in the *sept6*-tMO (70.0%; $n = 29$) and *sept6*-sMO (57.7%; $n = 26$) morphants (Fig. 5D). When the embryos were coinjected with *sept6*-MO and *sept6* mRNA, only 36.0% of the *sept6*-tMO ($n = 25$) and 26.1% of the *sept6*-sMO ($n = 23$) morphants exhibited abnormal patterns of *spaw* expression.

In the control embryos, *lefty1* and *lefty2* were also expressed at the left side of the LPM (Fig. 5E, I, and M). In contrast, the expression of these genes occurred at the middle or right side of the LPM in the *sept6* morphants (Fig. 5F, G, J, K, and N). Fifty-two percent of the *sept6*-tMO ($n = 25$) and 55.2% of the *sept6*-sMO ($n = 29$) morphants displayed abnormal patterning of *lefty1*. Coinjection of *sept6* mRNA and *sept6*-MO into the embryos partially rescued the patterning defects of *lefty1* to 28.0% ($n = 25$, *sep6*-tMO) and 25.0% ($n = 28$, *sept6*-sMO), respectively (Fig. 5H). Similar defects and partial rescues were also observed for *lefty2* in the *sept6* morphants (Fig. 5L). In this experiment, *no tail* (*ntl*) was used to mark the midline of the embryos. Together, these data indicate that *sept6* is required LR asymmetry of nodal signaling during the segmentation stage.

***sept6* regulates KV ciliogenesis.** KV is a ciliated, fluid-filled organ in zebrafish that plays a critical role in nodal signaling and LR development (38, 60, 61). Because septins are known to localize at the base of primary cilia and affect cilium-based signaling in other vertebrate cells (13, 25), we reasoned that *sept6* may affect LR asymmetry in zebrafish by regulating ciliogenesis in KV. We tested this hypothesis by examining KV formation and its ciliogenesis with the KV-specific marker *charon* and an antibody against acetylated α-tubulin, which is the major structural component of KV cilia. WISH analysis showed that the overall architecture of KV in the *sept6* morphants was largely unaffected compared with the control embyos (Fig. 6A to C). However, both the number and the length of KV cilia in the *sept6* morphants were significantly reduced from those in the control embryos at the 8-ss stage ($P < 0.001$) (Fig. 6D to H). The mean length of cilia was

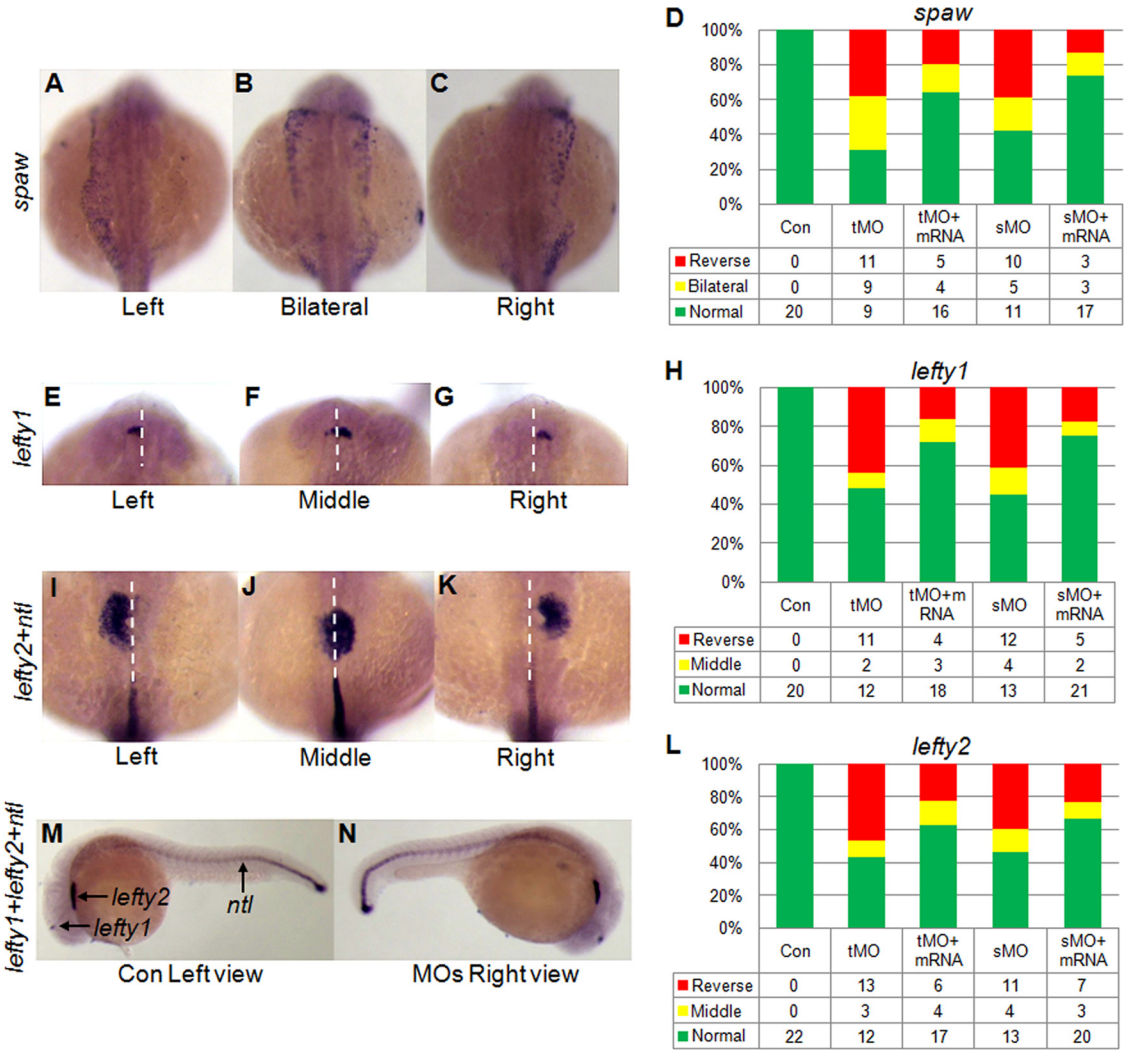

FIG 5 Knockdown of *sept6* causes defects in the expression patterns of nodal pathway genes in the LPM. In the control embryos, *spaw* (A), *lefty1* (E), and *lefty2* (I) were expressed at the left side of the midline at 20 hpf, while bilateral or middle (B, F, and J) and inverted (C, G, and K) expression patterns of these genes were observed in the *sept6* morphants. Percentages of different patterns in the control embryos, *sept6* morphants, and rescued embryos were quantified and are presented in the bar charts (D, H, and L). (M and N) WISH analysis of *left1*, *lefty2*, and *ntl* in a control embryo (M, lateral view with the anterior at the left side) and a morphant (N, lateral view with the anterior at the right side).

4.33 ± 0.11 μm (mean ± standard deviation) for the control embryos (n_{embryo} = 10, n_{cilia} = 135), 2.73 ± 0.08 μm (n_{embryo} = 10, n_{cilia} = 127) for the *sept6*-tMO morphants, and 2.90 ± 0.08 μm (n_{embryo} = 10, n_{cilia} = 129) for the sMO morphants. The number of cilia per KV was also significantly ($P < 0.001$) reduced in the *sept6*-tMO (24.56 ± 2.80; n_{embryo} = 10) and *sept6*-sMO (28.33 ± 1.6; n_{embyo} = 10) morphants compared with the control embryos (40.10 ± 3.6; n_{embryo} = 10). These data suggest that *sept6* plays a critical role in KV ciliogenesis.

FCF, a septin inhibitor (52, 53), is known to alter septin assembly and organization in mammalian cells (52). When wild-type embryos were cultured in the presence of 150 μM FCF from 70% epiboly to the prim-5 stage, 80.0% of the FCF-treated embryos (n = 30) displayed a defect in liver positioning, whereas 3‰ of DMSO-treated control embryos did not display such a phenotype (Fig. 6I and J). FCF-treated embryos also showed an apparent decrease in the number and length of KV cilia at the 8-ss stage (Fig. 6K and L). These data suggest that septin assembly and/or organization are involved in KV ciliogenesis, which further corroborates the role of *sept6* in this process.

Dorsal forerunner cells (DFCs)/KV cells are known to play a central role in the development of LR asymmetry (37–39, 61). To determine whether *sept6* affects LR asymmetry through these cells or other mechanisms, we injected embryos with *sept6*-tMO at the 256-cell stage. At the 256-cell stage, the bridge between yolk and DFCs/KV cells is open while other bridges between yolk and embryonic cells are closed, so that tMO can enter the progenitors of the DFCs through the cytoplasmic bridge without entering most other embryonic cells (Fig. 7A) (61). WISH analysis using the probe of *sox17*, which marks the DFCs and endoderm cells during the blastula stage, indicated that DFC migration and cohesion were not affected (Fig. 7B and C). However, the laterality defect of visceral organs was increased in the morphants compared with the control embryos at 2 dpf (Fig. 7D and E), whereas global defects, such as curvature of the body displayed by embryos injected with *sept6*-MO at the one-cell stage, were not observed (Fig. 7F to H).

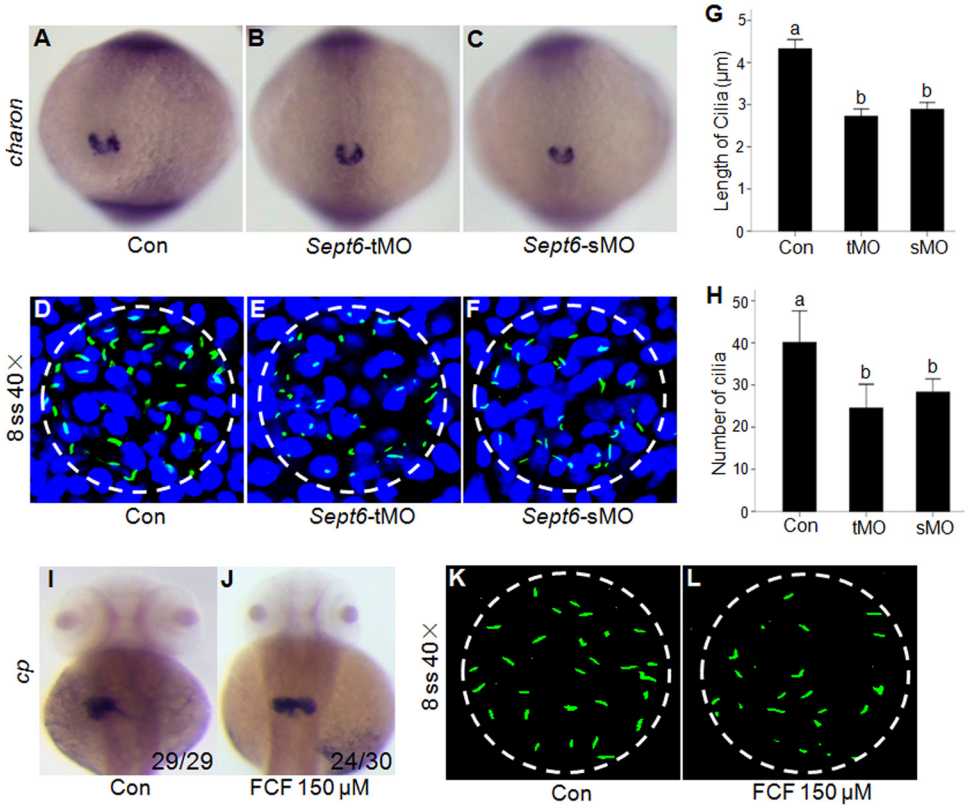

FIG 6 Knockdown of *sept6* causes defects in KV ciliogenesis. (A to C) Representative images of *charon* expression in KV in control embryos (A), *sept6*-tMO morphants (B), and sMO morphants (C). (D to F) Cilia in the KV were visualized by immunofluorescence of acetylated α-tubulin in the control embryos (D), *sept6*-tMO morphants (E), and sMO morphants (F). (G and H) Bar charts represent the quantification and statistical analyses of cilia length (G) and numbers (H) at the 8-ss stage. The letters a and b represent statistically significant differences ($P < 0.001$, calculated by using Student's *t* test). (I and J) FCF treatment caused defects in LR patterning of the liver, as demonstrated by WISH analysis of the liver-specific marker *cp* at 50 hpf in the control (I) and FCF-treated (J) embryos. (K and L) Immunofluorescence of acetylated α-tubulin in the control (K) and FCF-treated (L) embryos. Nuclear DNA was stained with 4′,6-diamidino-2-phenylindole, and the KV is circled (D to F, K, and L).

These data suggest that *sept6* likely affects ciliogenesis and LR patterning of visceral organs directly, through DFCs/KV cells.

***sept6* is required for ciliogenesis in the pronephric duct and neural tube.** To investigate whether ciliogenesis in other tissues is also affected by *sept6* knockdown, we examined ciliogenesis in the pronephros and neural tube, where *sept6* RNA was detected. The pronephros consists of a glomerulus (Fig. 8A, arrow) and a pair of ciliated pronephric tubules (Fig. 8A, green circles) and ducts

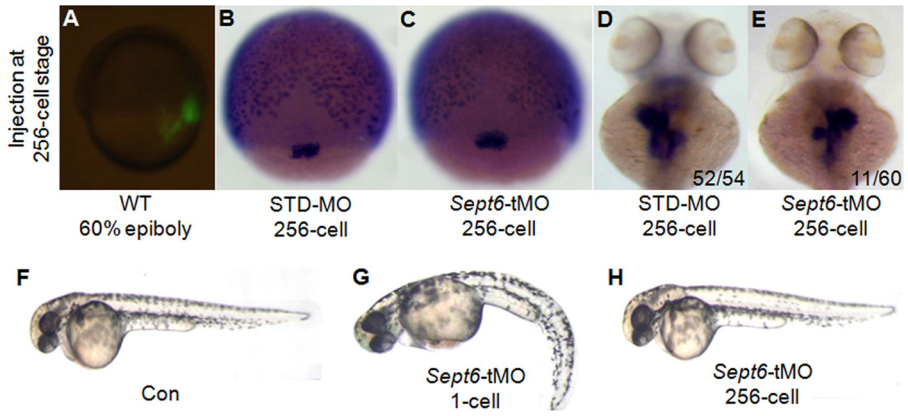

FIG 7 Specific knockdown of SEPT6 in DFCs/KV cells causes specific defects in LR patterning. (A) Representative image of an embryo after injection of fluorescence-labeled membrane dye at the 256-cell stage. This labeling experiment demonstrated that the injection was targeted to the intended location. (B and C) DFC architecture was not affected during the gastrula stage in the embryos injected with *sept6*-tMO at the 256-cell stage compared with the control embryos. (D and E) *sept6*-tMO injection at the 256-cell stage caused inverted patterning of visceral organs (E), in contrast to std-MO injection (D). (F to H) Similar to the control embryos (F), embryos injected with *sept6*-tMO at the 256-cell stage (H) showed fewer global defects than those injected at the 1-cell stage (G).

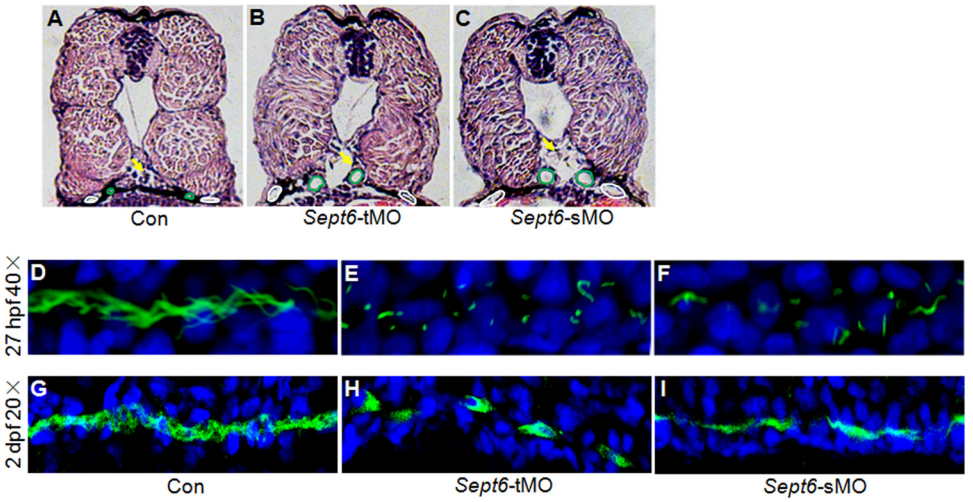

FIG 8 Knockdown of *sept6* causes defects in ciliogenesis and the development of zebrafish pronephros. (A to C) Hematoxylin and eosin (HE) staining of cross-sections of the 72-hpf control embryos (A), *sept6*-tMO morphants (B), and sMO morphants (C). Arrows, glomerulus; green circles, pronephric tubules; white circles, pronephric ducts. (D to I) Whole-mount immunofluorescence of acetylated α-tubulin in the cilia of the pronephric ducts at 27 hpf (D to F) and at 2 dpf (G to I) in the control embryos (D and G), *sept6*-tMO morphants (E and H), and *sept6*-sMO morphants (F and I).

(Fig. 8A, white circles). Histological sections of 3-dpf embryos showed dilation of the pronephric tubules and ducts in the *sept6* morphants (Fig. 8B and C). Such phenotypes have been associated with defective ciliogenesis before (32–36). Consistent with this notion, we found that the number and length of cilia in the pronephric ducts were significantly reduced in the *sept6* morphants at 27 hpf and 2 dpf (Fig. 8D to I).

Previous studies indicate that cilia play an essential role in the transduction of Shh signaling, which specifies neuronal cell fates in the neural tube (62–66). Several Shh pathway components, including PATCH 1 (the receptor for Shh) and GLI (transcription factors), are present in the cilia (67, 68). Organisms with mutations or morphants of genes required for ciliogenesis are often defective in Shh signaling (62–64, 69). We found that ciliogenesis in the neural tube was significantly compromised in the *sept6* morphants (Fig. 9A to C). As expected, the expression levels of the Shh target genes *gli1*, *nkx2.2*, and *ptch1* were reduced in the morphants (Fig. 9D and G to L). In contrast, the expression of *shh* was unaffected (Fig. 9D to F). These data suggest that *sept6* is involved in cilium-based Shh signaling. Collectively, our results demonstrate that *sept6* plays a role in ciliogenesis in the pronephros and neural tube in zebrafish.

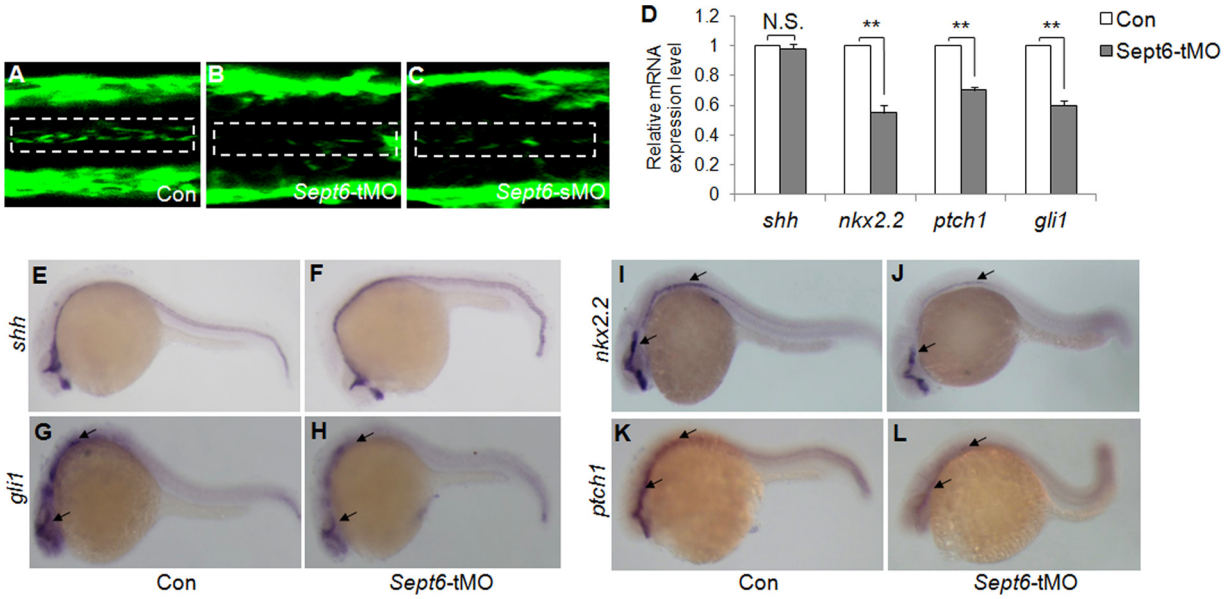

FIG 9 *sept6* is required for ciliogenesis and the Shh signaling pathway in the zebrafish neural tube. (A to C) Immunofluorescence analysis of acetylated α-tubulin on longitudinal cryosections of embryos at 2 dpf from control embryos (A), *sept6*-tMO morphants (B), and sMO morphants (C). The cilium area in the neural tubes is boxed. (D to L) WISH and real-time PCR analysis of Shh signaling components. Expression of *shh* was comparable in the control embryos and the morphants at 24 hpf (D, E, and F). In contrast, the expression levels of *gli1*, *nkx2.2*, and *ptch1* in the central nervous system of *sept6*-tMO morphants (D, H, J, and L) were reduced in comparison to the control embryos (D, G, I, and K). **, $P \leq 0.01$; N.S., not significant. Arrows (G to L) indicate the central nervous system.

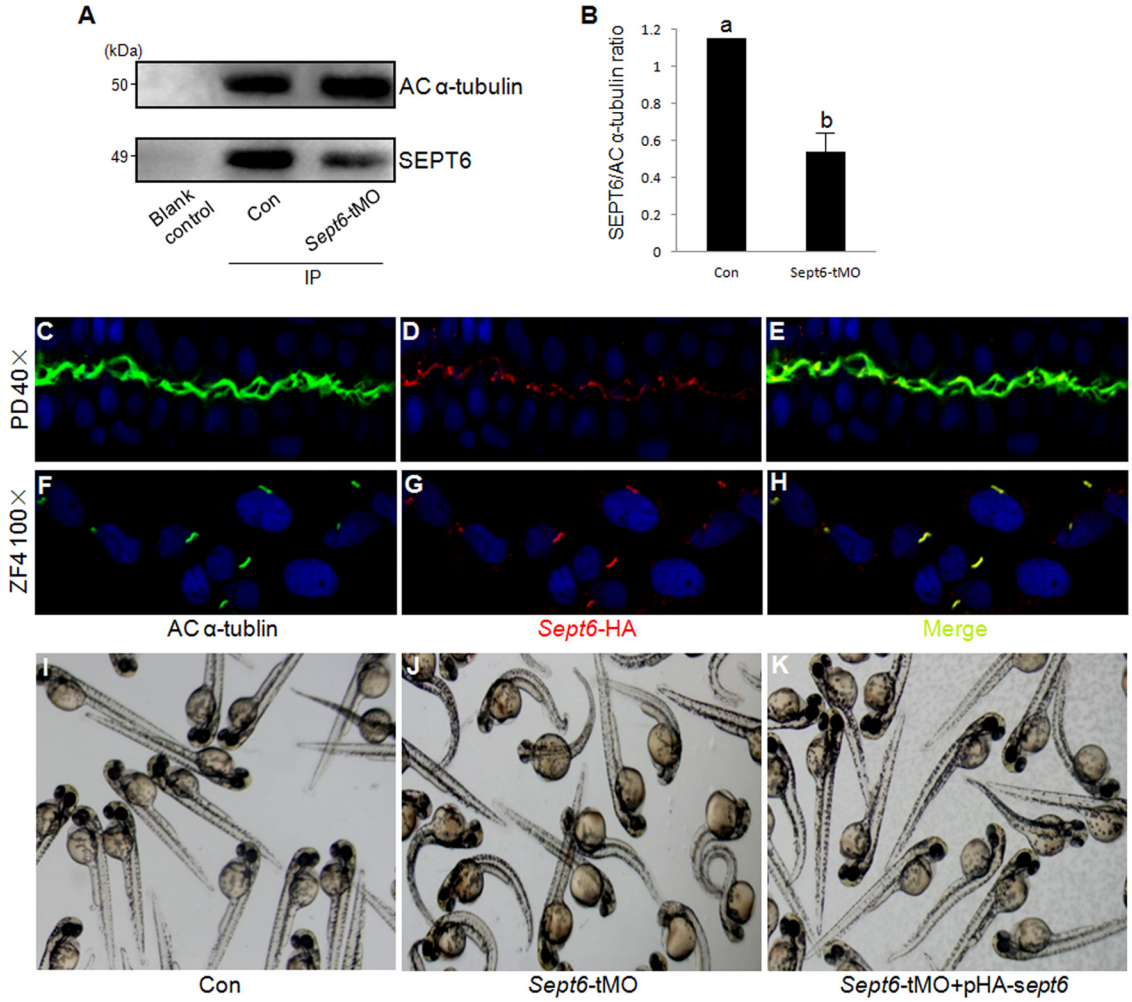

FIG 10 SEPT6 associates with acetylated α-tubulin in cilia. (A) The endogenous SEPT6 coimmunoprecipitates with acetylated (AC) α-tubulin. Briefly, lysates from embryos were immunoprecipitated with resin beads coated with anti-acetylated α-tubulin. The levels of acetylated α-tubulin (upper panel) and SEPT6 (lower panel) in the precipitates were analyzed by Western blotting using antibodies against each protein. Lane 1, blank control sample; lane 2, control embryos; lane 3, *sept6*-tMO morphants. (B) Quantification of SEPT6 that coimmunoprecipitated with acetylated α-tubulin (α-tubulin also serving as the normalization standard) from the control embryos and *sept6*-tMO morphants. The letters a and b indicate statistically significant differences ($P < 0.001$, calculated by using Student's *t* test). (C to E) Localization of HA-SEPT6 in relation to the acetylated microtubules in the cilia of the pronephric ducts in embryos injected with p*HA-sept6*, visualized by double staining with antibodies against acetylated α-tubulin (C) and the HA tag (D). Acetylated α-tubulin and SEPT6 localizations are merged in panel E. (F to H) Colocalization of HA-SEPT6 with acetylated α-tubulin in the cilia of p*HA-sept6*-transfected ZF4 cells. Acetylated α-tubulin (F) and HA-SEPT6 (G) showed colocalization as indicated in the merged image (H). (I to K) Coinjection of the *HA-sept6* plasmid at 15 ng/μl effectively rescued the global defects of embryos that were caused by *sept6*-tMO.

Sept6 associates with acetylated α-tubulin in cilia. To determine how SEPT6 affects ciliogenesis in zebrafish, we first examined whether SEPT6 is associated with acetylated α-tubulin, a major component of cilia. We found that the endogenous SEPT6 was effectively coimmunoprecipitated with acetylated α-tubulin in embryos at the 8-ss stage, when ciliogenesis is occurring in KV, and this association was significantly reduced in the *sept6*-tMO morphants in comparison to the control embryos ($P < 0.001$) (Fig. 10A and B). Because the rabbit antibody against human SEPT6 did not work well in our whole-mount immunofluorescence experiments, we determined the localization of HA-tagged SEPT6, which is carried on a plasmid and expressed from the CMV promoter, in relation to that of cilia in the pronephric ducts of embryos at 27 hpf as well as in the ZF4 cells. Surprisingly, in both the pronephric ducts and the ZF4 cells, HA-SEPT6 colocalized with acetylated α-tubulin in cilia (Fig. 10C to H). We also demonstrated that the HA-SEPT6 construct was functional, as it effectively rescued the global defects of the *sept6* morphants (Fig. 10I to K). Taken together, these data suggest that SEPT6 likely affects ciliogenesis in zebrafish via its association with acetylated α-tubulin along the axoneme in cilia.

DISCUSSION

In this study, we have shown that *sept6* is expressed in the ciliated organs, including KV, the pronepheros, and the neural tube in zebrafish. SEPT6 associates with acetylated α-tubulin in the axoneme of cilia of pronephric ducts and ZF4 cells. This defines a novel pattern of SEPT6 localization in cilia that is distinct from the ring-like structure formed at the base of primary cilia by SEPT7 in *Xenopus* multiciliated cells (25) and SEPT2 in mouse IMCD3 cells

(13). Knockdown of *sept6* in zebrafish causes profound defects in ciliogenesis, resulting in changes in the function of the ciliated organs mentioned above. Thus, our study, for the first time, has defined a cellular and developmental role for SEPT6 in vertebrates.

LR patterning is an important developmental issue that has been analyzed extensively in different vertebrate systems (39, 40, 57, 70). In zebrafish, monocilia in KV are known to generate a counterclockwise fluid flow that is critical for nodal/spaw signaling and the development of LR asymmetry (36, 37, 60). In this study, we found that global or KV-specific knockdown of *sept6* resulted in defective ciliogenesis in KV. Consequently, nodal signaling and LR patterning of visceral organs are compromised. Thus, SEPT6 likely regulates organ laterality through KV ciliogenesis.

SEPT6 also regulates ciliogenesis in the pronephros and neural tube in zebrafish. Knockdown of *sept6* caused cyst formation and dilation of pronephric ducts and tubules in the pronephros. Knockdown of *sept6* also caused defective ciliogenesis in the neural tube and, consequently, compromised the cilium-based Shh signaling. All these phenotypes observed in the *sept6* morphants are strikingly similar to those displayed by mouse mutants or zebrafish morphants deficient in ciliary components, such as IFT, PKD, and ARL13b (36, 71, 72). Thus, our study strongly implicates SEPT6 in the regulation of ciliogenesis in multiple organs during zebrafish development.

All septins are known to form hetero-oligomeric complexes that can further assemble into filaments and other higher-order structures, such as rings and hourglasses (15). Despite extensive characterization of some septin complexes *in vitro*, the composition and size of septin complexes in specific cell types or tissues remain largely unknown. While our manuscript was under revision, the mammalian SEPT2/7/9 complex was reported to colocalize with ciliary microtubules and to control ciliary length in RPE cells (26). In addition, FCF, an inhibitor of septin assembly and organization, affects ciliogenesis and LR patterning of visceral organs (this study). Based on these observations, it is tempting to speculate that SEPT6 controls ciliogenesis in zebrafish by forming a complex with other septins.

Because of the complexity and plasticity in the assembly and function of septin complexes and the potential functional overlap between different septins, it is difficult, if not impossible, to predict whether a specific septin knockout or knockdown would produce certain phenotypes. For example, mammalian SEPT2/6/7 and SEPT2/6/7/9 complexes have been well characterized *in vitro* (17). However, mouse knockout studies have indicated that deletion of *sept7* or *sept9* causes embryonic lethality, while deletion of *sept6* produces no detectable phenotypes (46). The underlying reason remains unknown. The difference in the requirement of specific septins for organismal survival is even more striking. For example, *CDC3* and *CDC12* are essential for the survival of the budding yeast *S. cerevisiae*, while their counterparts, *SPN1* and *SPN4*, are totally dispensable for the survival of the fission yeast *Schizosaccharomyces pombe* (9, 73–75). In light of these observations, it is not surprising that *sept6* knockdown in zebrafish produced drastic phenotypes whereas *sept6* knockout mice display no obvious defects. Many outstanding questions regarding septin structure and function remain unanswered. Our work here is intended to establish zebrafish as a model in parallel with other systems in exploring the role of vertebrate septins in cellular and developmental processes.

ACKNOWLEDGMENTS

We thank Julia Hanna for carefully reading the manuscript.

Work in the Yin lab was supported by the National Basic Research Program of China (973 Program, 2010CB126302) and the National Natural Science Foundation of China (30925027 and 30871402). Work in the Bi lab was supported by grants GM59216 and GM87365 from the U.S. National Institutes of Health.

REFERENCES

1. **Cid VJ, Adamikova L, Sanchez M, Molina M, Nombela C.** 2001. Cell cycle control of septin ring dynamics in the budding yeast. Microbiology **147:**1437–1450.
2. **Kartmann B, Roth D.** 2001. Novel roles for mammalian septins: from vesicle trafficking to oncogenesis. J. Cell Sci. **114:**839–844.
3. **Wasik AA, Polianskyte-Prause Z, Dong MQ, Shaw AS, Yates JR, III, Farquhar MG, Lehtonen S.** 2012. Septin 7 forms a complex with CD2AP and nephrin and regulates glucose transporter trafficking. Mol. Biol. Cell **23:**3370–3379. http://dx.doi.org/10.1091/mbc.E11-12-1010.
4. **Estey MP, Di Ciano-Oliveira C, Froese CD, Bejide MT, Trimble WS.** 2010. Distinct roles of septins in cytokinesis: SEPT9 mediates midbody abscission. J. Cell Biol. **191:**741–749. http://dx.doi.org/10.1083/jcb.201006031.
5. **Wloka C, Nishihama R, Onishi M, Oh Y, Hanna J, Pringle JR, Krauss M, Bi E.** 2011. Evidence that a septin diffusion barrier is dispensable for cytokinesis in budding yeast. Biol. Chem. **392:**813–829. http://dx.doi.org/10.1515/BC.2011.083.
6. **Finger FP, Kopish KR, White JG.** 2003. A role for septins in cellular and axonal migration in C. elegans. Dev. Biol. **261:**220–234. http://dx.doi.org/10.1016/S0012-1606(03)00296-3.
7. **Gilden JK, Peck S, Chen YC, Krummel MF.** 2012. The septin cytoskeleton facilitates membrane retraction during motility and blebbing. J. Cell Biol. **196:**103–114. http://dx.doi.org/10.1083/jcb.201105127.
8. **Spiliotis ET, Kinoshita M, Nelson WJ.** 2005. A mitotic septin scaffold required for mammalian chromosome congression and segregation. Science **307:**1781–1785. http://dx.doi.org/10.1126/science.1106823.
9. **Oh Y, Bi E.** 2011. Septin structure and function in yeast and beyond. Trends Cell Biol. **21:**141–148. http://dx.doi.org/10.1016/j.tcb.2010.11.006.
10. **Kissel H, Georgescu MM, Larisch S, Manova K, Hunnicutt GR, Steller H.** 2005. The Sept4 septin locus is required for sperm terminal differentiation in mice. Dev. Cell **8:**353–364. http://dx.doi.org/10.1016/j.dev.cell.2005.01.021.
11. **Kwitny S, Klaus AV, Hunnicutt GR.** 2010. The annulus of the mouse sperm tail is required to establish a membrane diffusion barrier that is engaged during the late steps of spermiogenesis. Biol. Reprod. **82:**669–678. http://dx.doi.org/10.1095/biolreprod.109.079566.
12. **Hu J, Bai X, Bowen JR, Dolat L, Korobova F, Yu W, Baas PW, Svitkina T, Gallo G, Spiliotis ET.** 2012. Septin-driven coordination of actin and microtubule remodeling regulates the collateral branching of axons. Curr. Biol. **22:**1109–1115. http://dx.doi.org/10.1016/j.cub.2012.04.019.
13. **Hu Q, Milenkovic L, Jin H, Scott MP, Nachury MV, Spiliotis ET, Nelson WJ.** 2010. A septin diffusion barrier at the base of the primary cilium maintains ciliary membrane protein distribution. Science **329:**436–439. http://dx.doi.org/10.1126/science.1191054.
14. **Xie Y, Vessey JP, Konecna A, Dahm R, Macchi P, Kiebler MA.** 2007. The GTP-binding protein Septin 7 is critical for dendrite branching and dendritic-spine morphology. Curr. Biol. **17:**1746–1751. http://dx.doi.org/10.1016/j.cub.2007.08.042.
15. **Mostowy S, Cossart P.** 2012. Septins: the fourth component of the cytoskeleton. Nat. Rev. Mol. Cell Biol. **13:**183–194. http://dx.doi.org/10.1038/nrm3284.
16. **Cao L, Ding X, Yu W, Yang X, Shen S, Yu L.** 2007. Phylogenetic and evolutionary analysis of the septin protein family in metazoan. FEBS Lett. **581:**5526–5532. http://dx.doi.org/10.1016/j.febslet.2007.10.032.
17. **Dolat L, Hu Q, Spiliotis ET.** 2014. Septin functions in organ system physiology and pathology. Biol. Chem. **395:**123–141. http://dx.doi.org/10.1515/hsz-2013-0233.
18. **Kinoshita M.** 2003. Assembly of mammalian septins. J. Biochem. **134:**491–496. http://dx.doi.org/10.1093/jb/mvg182.

19. **Low C, Macara IG.** 2006. Structural analysis of septin 2, 6, and 7 complexes. J. Biol. Chem. **281:**30697–30706. http://dx.doi.org/10.1076/jbc.M605179200.
20. **Sirajuddin M, Farkasovsky M, Hauer F, Kuhlmann D, Macara IG, Weyand M, Stark H, Wittinghofer A.** 2007. Structural insight into filament formation by mammalian septins. Nature **449:**311–315. http://dx.doi.org/10.1038/nature06052.
21. **Kim MS, Froese CD, Estey MP, Trimble WS.** 2011. SEPT9 occupies the terminal positions in septin octamers and mediates polymerization-dependent functions in abscission. J. Cell Biol. **195:**815–826. http://dx.doi.org/10.1083/jcb.201106131.
22. **Sellin ME, Sandblad L, Stenmark S, Gullberg M.** 2011. Deciphering the rules governing assembly order of mammalian septin complexes. Mol. Biol. Cell **22:**3152–3164. http://dx.doi.org/10.1091/mbc.E11-03-0253.
23. **Bertin A, McMurray MA, Grob P, Park SS, Garcia G, 3rd, Patanwala I, Ng HL, Alber T, Thorner J, Nogales E.** 2008. Saccharomyces cerevisiae septins: supramolecular organization of heterooligomers and the mechanism of filament assembly. Proc. Natl. Acad. Sci. U. S. A. **105:**8274–8279. http://dx.doi.org/10.1073/pnas.0803330105.
24. **McMurray MA, Bertin A, Garcia G, III, Lam L, Nogales E, Thorner J.** 2011. Septin filament formation is essential in budding yeast. Dev. Cell **20:**540–549. http://dx.doi.org/10.1016/devcel.2011.02.004.
25. **Kim SK, Shindo A, Park TJ, Oh EC, Ghosh S, Gray RS, Lewis RA, Johnson CA, Attie-Bittach T, Katsanis N, Wallingford JB.** 2010. Planar cell polarity acts through septins to control collective cell movement and ciliogenesis. Science **329:**1337–1340. http://dx.doi.org/10.1126/science.1191184.
26. **Ghossoub R, Hu Q, Failler M, Rouyez MC, Spitzbarth B, Mostowy S, Wolfrum U, Saunier S, Cossart P, Jamesnelson W, Benmerah A.** 2013. Septins 2, 7 and 9 and MAP4 colocalize along the axoneme in the primary cilium and control ciliary length. J. Cell Sci. **126:**2583–2594. http://dx.doi.org/10.1242/jcs.111377.
27. **Baker K, Beales PL.** 2009. Making sense of cilia in disease: the human ciliopathies. Am. J. Med. Genet. C Semin. Med. Genet. **151C:**281–295. http://dx.doi.org/10.1002/ajmg.c.30231.
28. **Gerdes JM, Davis EE, Katsanis N.** 2009. The vertebrate primary cilium in development, homeostasis, and disease. Cell **137:**32–45. http://dx.doi.org/10.1016/j.cell.2009.03.023.
29. **Afzelius BA.** 2004. Cilia-related diseases. J. Pathol. **204:**470–477. http://dx.doi.org/10.1002/path.1652.
30. **Barr MM, DeModena J, Braun D, Nguyen CQ, Hall DH, Sternberg PW.** 2001. The Caenorhabditis elegans autosomal dominant polycystic kidney disease gene homologs lov-1 and pkd-2 act in the same pathway. Curr. Biol. **11:**1341–1346. http://dx.doi.org/10.1016/S0960-9822(01)00423-7.
31. **Blacque OE, Reardon MJ, Li C, McCarthy J, Mahjoub MR, Ansley SJ, Badano JL, Mah AK, Beales PL, Davidson WS, Johnsen RC, Audeh M, Plasterk RH, Baillie DL, Katsanis N, Quarmby LM, Wicks SR, Leroux MR.** 2004. Loss of C. elegans BBS-7 and BBS-8 protein function results in cilia defects and compromised intraflagellar transport. Genes Dev. **18:**1630–1642. http://dx.doi.org/10.1101/gad.1194004.
32. **Fan Y, Esmail MA, Ansley SJ, Blacque OE, Boroevich K, Ross AJ, Moore SJ, Badano JL, May-Simera H, Compton DS, Green JS, Lewis RA, van Haelst MM, Parfrey PS, Baillie DL, Beales PL, Katsanis N, Davidson WS, Leroux MR.** 2004. Mutations in a member of the Ras superfamily of small GTP-binding proteins causes Bardet-Biedl syndrome. Nat. Genet. **36:**989–993. http://dx.doi.org/10.1038/ng1414.
33. **Pazour GJ, San Agustin JT, Follit JA, Rosenbaum JL, Witman GB.** 2002. Polycystin-2 localizes to kidney cilia and the ciliary level is elevated in *orpk* mice with polycystic kidney disease. Curr. Biol. **12:**R378–R380. http://dx.doi.org/10.1016/S0960-9822(02)00877-1.
34. **Sun Z, Amsterdam A, Pazour GJ, Cole DG, Miller MS, Hopkins N.** 2004. A genetic screen in zebrafish identifies cilia genes as a principal cause of cystic kidney. Development **131:**4085–4093. http://dx.doi.org/10.1242/dev.01240.
35. **Yoder BK, Tousson A, Millican L, Wu JH, Bugg CE, Jr, Schafer JA, Balkovetz DF.** 2002. Polaris, a protein disrupted in *orpk* mutant mice, is required for assembly of renal cilium. Am. J. Physiol. Renal Physiol. **282:**F541–F552. http://dx.doi.org/10.1152/ajprenal.00273.2001.
36. **Kramer-Zucker AG, Olale F, Haycraft CJ, Yoder BK, Schier AF, Drummond IA.** 2005. Cilia-driven fluid flow in the zebrafish pronephros, brain and Kupffer's vesicle is required for normal organogenesis. Development **132:**1907–1921. http://dx.doi.org/10.1242/dev.01772.
37. **Hirokawa N, Tanaka Y, Okada Y, Takeda S.** 2006. Nodal flow and the generation of left-right asymmetry. Cell **125:**33–45. http://dx.doi.org/10.1016/j.cell.2006.03.002.
38. **Essner JJ, Amack JD, Nyholm MK, Harris EB, Yost HJ.** 2005. Kupffer's vesicle is a ciliated organ of asymmetry in the zebrafish embryo that initiates left-right development of the brain, heart and gut. Development **132:**1247–1260. http://dx.doi.org/10.1242/dev.01663.
39. **Yost HJ.** 2003. Left-right asymmetry: nodal cilia make and catch a wave. Curr. Biol. **13:**R808–R809. http://dx.doi.org/10.1016/j.cub.2003.09.051.
40. **Oki S, Kitajima K, Marques S, Belo JA, Yokoyama T, Hamada H, Meno C.** 2009. Reversal of left-right asymmetry induced by aberrant Nodal signaling in the node of mouse embryos. Development **136:**3917–3925. http://dx.doi.org/10.1242/dev.039305.
41. **Hu M, Easter SS.** 1999. Retinal neurogenesis: the formation of the initial central patch of postmitotic cells. Dev. Biol. **207:**309–321.
42. **Jing X, Malicki J.** 2009. Zebrafish ale oko, an essential determinant of sensory neuron survival and the polarity of retinal radial glia, encodes the p50 subunit of dynactin. Development **136:**2955–2964. http://dx.doi.org/10.1242/dev.037739.
43. **Khanna H, Davis EE, Murga-Zamalloa CA, Estrada-Cuzcano A, Lopez I, den Hollander AI, Zonneveld MN, Othman MI, Waseem N, Chakarova CF, Maubaret C, Diaz-Font A, MacDonald I, Muzny DM, Wheeler DA, Morgan M, Lewis LR, Logan CV, Tan PL, Beer MA, Inglehearn CF, Lewis RA, Jacobson SG, Bergmann C, Beales PL, Attie-Bitach T, Johnson CA, Otto EA, Bhattacharya SS, Hildebrandt F, Gibbs RA, Koenekoop RK, Swaroop A, Katsanis N.** 2009. A common allele in RPGRIP1L is a modifier of retinal degeneration in ciliopathies. Nat. Genet. **41:**739–745. http://dx.doi.org/10.1038/ng.366.
44. **Green JA, Mykytyn K.** 2010. Neuronal ciliary signaling in homeostasis and disease. Cell. Mol. Life Sci. **67:**3287–3297. http://dx.doi.org/10.1007/s00018-010-0425-4.
45. **Slater DJ, Hilgenfeld E, Rappaport EF, Shah N, Meek RG, Williams WR, Lovett BD, Osheroff N, Autar RS, Ried T, Felix CA.** 2002. MLL-SEPTIN6 fusion recurs in novel translocation of chromosomes 3, X, and 11 in infant acute myelomonocytic leukaemia and in t(X;11) in infant acute myeloid leukaemia, and MLL genomic breakpoint in complex MLL-SEPTIN6 rearrangement is a DNA topoisomerase II cleavage site. Oncogene **21:**4706–4714. http://dx.doi.org/10.1038/sj.onc.1205572.
46. **Ono R, Ihara M, Nakajima H, Ozaki K, Kataoka-Fujiwara Y, Taki T, Nagata K, Inagaki M, Yoshida N, Kitamura T, Hayashi Y, Kinoshita M, Nosaka T.** 2005. Disruption of Sept6, a fusion partner gene of MLL, does not affect ontogeny, leukemogenesis induced by MLL-SEPT6, or phenotype induced by the loss of Sept4. Mol. Cell. Biol. **25:**10965–10978. http://dx.doi.org/10.1128/MCB.25.24.10965-10978.2005.
47. **Westerfield M.** 2000. The zebrafish book, a guide for the laboratory use of zebrafish (Danio rerio), 4th ed. University of Oregon Press, Eugene, OR.
48. **Kimmel CB, Ballard WW, Kimmel SR, Ullmann B, Schilling TF.** 1995. Stages of embryonic development of the zebrafish. Dev. Dyn. **203:**253–310.
49. **Thisse C, Thisse B.** 2008. High-resolution in situ hybridization to whole-mount zebrafish embryos. Nat. Protoc. **3:**59–69. http://dx.doi.org/10.1038/nprot.2007.514.
50. **Jaffe KM, Thiberge SY, Bisher ME, Burdine RD.** 2010. Imaging cilia in zebrafish. Methods Cell Biol. **97:**415–435. http://dx.doi.org/10.1016/S0091-679X(10)97022-2.
51. **Malicki J, Avanesov A, Li J, Yuan S, Sun Z.** 2011. Analysis of cilia structure and function in zebrafish. Methods Cell Biol. **101:**39–74. http://dx.doi.org/10.1016/B978-0-12-00003-7.
52. **Hu Q, Nelson WJ, Spiliotis ET.** 2008. Forchlorfenuron alters mammalian septin assembly, organization, and dynamics. J. Biol. Chem. **283:**29563–29571. http://dx.doi.org/10.1074/jbc.M8049562200.
53. **Iwase M, Okada S, Oguchi T, Toh-e A.** 2004. Forchlorfenuron, a phenylurea cytokinin, disturbs septin organization in Saccharomyces cerevisiae. Genes Genet. Syst. **79:**199–206. http://dx.doi.org/10.1266/ggs.79.199.
54. **Bourne HR, Sanders DA, McCormick F.** 1991. The GTPase superfamily: conserved structure and molecular mechanism. Nature **349:**117–127.
55. **Pan F, Malmberg RL, Momany M.** 2007. Analysis of septins across kingdoms reveals orthology and new motifs. BMC Evol. Biol. **7:**103. http://dx.doi.org/10.1186/1471-2148-7-103.
56. **Versele M, Gullbrand B, Shulewitz MJ, Cid VJ, Bahmanyar S, Chen RE, Barth P, Alber T, Thorner J.** 2004. Protein-protein interactions governing septin heteropentamer assembly and septin filament organization in

Saccharomyces cerevisiae. Mol. Biol. Cell **15:**4568–4583. http://dx.doi.org/10.1091/mbc.E04-40-0330.
57. **Tsikolia N, Schroder S, Schwartz P, Viebahn C.** 2012. Paraxial left-sided nodal expression and the start of left-right patterning in the early chick embryo. Differentiation **84:**380–391. http://dx.doi.org/10.1016/j.diff.2012.09.011.
58. **Long S, Ahmad N, Rebagliati M.** 2003. The zebrafish nodal-related gene southpaw is required for visceral and diencephalic left-right asymmetry. Development **130:**2303–2316. http://dx.doi.org/10.1242/dev.00436.
59. **Ahmad N, Long S, Rebagliati M.** 2004. A southpaw joins the roster: the role of the zebrafish nodal-related gene southpaw in cardiac LR asymmetry. Trends Cardiovasc. Med. **14:**43–49. http://dx.doi.org/10.1016/j.tcm.2003.11.001.
60. **Bisgrove BW, Essner JJ, Yost HJ.** 2000. Multiple pathways in the midline regulate concordant brain, heart and gut left-right asymmetry. Development **127:**3567–3579.
61. **Wang G, Yost HJ, Amack JD.** 2013. Analysis of gene function and visualization of cilia-generated fluid flow in Kupffer's vesicle. J. Vis. Exp. **73:**e50038. http://dx.doi.org/10.3791/50038.
62. **Murdoch JN, Copp AJ.** 2010. The relationship between sonic Hedgehog signaling, cilia, and neural tube defects. Birth Defects Res. A Clin. Mol. Teratol. **88:**633–652. http://dx.doi.org/10.1002/bdra.20686.
63. **Caspary T, Larkins CE, Anderson KV.** 2007. The graded response to Sonic Hedgehog depends on cilia architecture. Dev. Cell **12:**767–778. http://dx.doi.org/10.1016/j.devcel.2007.03.004.
64. **Liu A, Wang B, Niswander LA.** 2005. Mouse intraflagellar transport proteins regulate both the activator and repressor functions of Gli transcription factors. Development **132:**3103–3111. http://dx.doi.org/10.1242/dev.01894.
65. **Briscoe J, Sussel L, Serup P, Hartigan-O'Connor D, Jessell TM, Rubenstein JL, Ericson J.** 1999. Homeobox gene Nkx2.2 and specification of neuronal identity by graded Sonic hedgehog signalling. Nature **398:**622–627.
66. **Barth KA, Wilson SW.** 1995. Expression of zebrafish nk2.2 is influenced by sonic hedgehog/vertebrate hedgehog-1 and demarcates a zone of neuronal differentiation in the embryonic forebrain. Development **121:**1755–1768.
67. **Rohatgi R, Milenkovic L, Scott MP.** 2007. Patched 1 regulates hedgehog signaling at the primary cilium. Science **317:**372–376. http://dx.doi.org/10.1126/science.1139740.
68. **Haycraft CJ, Banizs B, Aydin-Son Y, Zhang Q, Michaud EJ, Yoder BK.** 2005. Gli2 and Gli3 localize to cilia and require the intraflagellar transport protein polaris for processing and function. PLoS Genet. **1**(4)**:**e53. http://dx.doi.org/10.1371/journal.pgen.0010053.
69. **Houde C, Dickinson RJ, Houtzager VM, Cullum R, Montpetit R, Metzler M, Simpson EM, Roy S, Hayden MR, Hoodless PA, Nicholson DW.** 2006. Hippi is essential for node cilia assembly and Sonic hedgehog signaling. Dev. Biol. **300:**523–533. http://dx.doi.org/10.1016/j.ydbio.2006.09.001.
70. **Raya A, Izpisua Belmonte JC.** 2008. Insights into the establishment of left-right asymmetries in vertebrates. Birth Defects Res. C Embryo Today **84:**81–94. http://dx.doi.org/10.1002/bdrc.20122.
71. **Kamura K, Kobayashi D, Uehara Y, Koshida S, Iijima N, Kudo A, Yokoyama T, Takeda H.** 2011. Pkd1l1 complexes with Pkd2 on motile cilia and functions to establish the left-right axis. Development **138:**1121–1129. http://dx.doi.org/10.1242/dev.058271.
72. **Duldulao NA, Lee S, Sun Z.** 2009. Cilia localization is essential for in vivo functions of the Joubert syndrome protein Arl13b/Scorpion. Development **136:**4033–4042. http://dx.doi.org/10.1242/dev.036350.
73. **Versele M, Thorner J.** 2005. Some assembly required: yeast septins provide the instruction manual. Trends Cell Biol. **15:**414–424. http://dx.doi.org/10.1016/j.tcb.2005.06.007.
74. **Longtine MS, DeMarini DJ, Valencik ML, Al-Awar OS, Fares H, De Virgilio C, Pringle JR.** 1996. The septins: roles in cytokinesis and other processes. Curr. Opin. Cell Biol. **8:**106–119.
75. **Wu JQ, Ye Y, Wang N, Pollard TD, Pringle JR.** 2010. Cooperation between the septins and the actomyosin ring and role of a cell-integrity pathway during cell division in fission yeast. Genetics **186:**897–915. http://dx.doi.org/10.1534/genetics.110.119842.